

Vessel-CAPTCHA: an efficient learning framework for vessel annotation and segmentation

Vien Ngoc Dang^a, Giuseppe Di Giacomo^{a,b}, Viola Marconetto^{a,b}, Prateek Mathur^a, Rosa Cortese^c, Marco Lorenzi^d, Ferran Prados^{e,c,f,g}, Maria A. Zuluaga^a

^aData Science Department, EURECOM, Sophia Antipolis, France

^bPolitecnico di Torino, Turin, Italy

^cQueen Square MS Centre, Dept of Neuroinflammation, UCL Queen Square Institute of Neurology, Faculty of Brain Sciences, University College London, UK

^dUniversité Côte d'Azur, Inria Sophia Antipolis, Epione Research Group, Valbonne, France

^eCentre for Medical Image Computing, Dept of Medical Physics and Bioengineering, University College London, UK

^fNational Institute for Health Research, University College London Hospitals, Biomedical Research Centre, London, UK

^ge-health Center, Universitat Oberta de Catalunya, Barcelona, Spain

ABSTRACT

The use of deep learning techniques for 3D brain vessel image segmentation has not been as widespread as for the segmentation of other organs and tissues. This can be explained by two factors. First, deep learning techniques tend to show poor performances at the segmentation of relatively small objects compared to the size of the full image. Second, due to the complexity of vascular trees and the small size of vessels, it is challenging to obtain the amount of annotated training data typically needed by deep learning methods. To address these problems, we propose a novel annotation-efficient deep learning vessel segmentation framework. The framework avoids pixel-wise annotations, only requiring patch-level labels to discriminate between vessel and non-vessel 2D patches in the training set, in a setup similar to the CAPTCHAs used to differentiate humans from bots in web applications. The user-provided annotations are used for two tasks: 1) to synthesize pixel-wise labels for vessels and background in each patch, which are used to train a segmentation network, and 2) to train a classifier network. The classifier network allows to generate additional weak patch labels, further reducing the annotation burden, and it acts as a noise filter for poor quality images. We use this framework for the segmentation of the cerebrovascular tree in Time-of-Flight angiography (TOF) and Susceptibility-Weighted Images (SWI). The results show that the framework achieves state-of-the-art accuracy, while reducing the annotation time by up to 80% with respect to learning-based segmentation methods using pixel-wise labels for training.

1. Introduction

The segmentation of the 3D brain vessel tree is a crucial task to the diagnosis, management, treatment and intervention of a wide range of conditions with a vast population-level impact (World Health Organization, 2020). Due to the high complexity of the cerebrovascular tree, its automatic extraction is a challenging task. Despite decades of research (Lesage et al., 2009; Moccia et al., 2018), the problem remains open.

With the advent of machine learning and, more precisely, deep learning techniques over the last decade (Litjens et al., 2017; Lundervold and Lundervold, 2019), image segmentation of organs and organs substructures, and lesions has reached state-of-the-art performance. This progress, however, has not been as fast in 3D brain vessel segmentation. Differently from the segmentation of other organs, there is no consolidated deep learning method which has reached human performance, and the vast majority of methods still rely on more classical tech-

Preprint submitted to Elsevier

niques (e.g. (Cetin and Unal, 2015; Klepaczko et al., 2016; Moriconi et al., 2019; Taher et al., 2020; Wang and Chung, 2020; Zhao et al., 2015; Zuluaga et al., 2014b)). This lag can be explained by two factors. First, deep learning techniques typically assume that the object to segment occupies an important part of the image (Deng et al., 2009; Shelhamer et al., 2017). On the opposite, vessels are relatively small objects within a large image volume (Livne et al., 2019). Secondly, deep learning techniques are well-known for being data greedy, as they require large annotated training datasets to avoid poor generalization. Due to the complexity of vascular trees and the small size of vessels, it is challenging to obtain sufficiently large high-quality annotated sets.

This work presents a novel framework to address the challenges faced by deep learning-based 3D vessel segmentation. Taking inspiration from Completely Automated Public Turing Test To Tell Computers and Humans Apart, better known as

CAPTCHA (von Ahn *et al.*, 2003), we initially divide the image volume into 2D image patches and we subsequently request the user to identify the patches containing a vessel or part of it. This task is common on websites to differentiate humans from bots, using image CAPTCHAs (von Ahn and Dabbish, 2004; Elson *et al.*, 2007) of natural images. This procedure, which we denote Vessel-CAPTCHA, simplifies the annotation process by requiring 2D patch tags indicating the presence of a vessel (a part of it, or multiple vessels) and, thus, avoiding pixel-wise annotations. The user-provided patch tags are subsequently used to synthesize a weak pixel-wise labeled training set in a self-supervised manner. These two sets are used to train the framework.

The proposed framework is composed of two networks: a segmentation network, which extracts vessels on a patch basis, to tackle the limitations of deep nets in the segmentation of small objects, and a classification network. The latter is used for two tasks. First, it allows to enlarge the labeled data without the need for further user-provided annotations. Second, it may act as a filter for noisy segmentations in low quality images. The final volumetric segmentation is obtained by concatenating the segmented patches. When the classification network is used as a filter, only the segmentations from patches identified as vessel patches are considered, while those classified as non-vessel patches are masked out.

1.1. Related Work

A comprehensive collection of methods and techniques for general vascular image segmentation is reviewed in (Lesage *et al.*, 2009; Moccia *et al.*, 2018), where they classify different segmentation frameworks according to their characteristic strategies. Classical approaches typically rely on hand-crafted features, with image intensity-derived (Taher *et al.*, 2020), and first (Law and Chung, 2008), second (Frangi *et al.*, 1998; Sato *et al.*, 1997) or higher order (Cetin and Unal, 2015) tensor-derived features among the most common. Feature extraction is followed by a vessel extraction scheme, which performs the final segmentation. Notable extraction schemes include deformable models (Klepaczko *et al.*, 2016; Zhao *et al.*, 2015),

voting (Zuluaga *et al.*, 2014b), tracking algorithms (Rempfler *et al.*, 2015; Robben *et al.*, 2016) and statistical approaches (Hassouna *et al.*, 2006). Their main drawbacks are two. First, these methods rely on hand-crafted features that need to be tuned, requiring high expertise to find a good set of parameters. Second, extraction schemes are not fully automatic: many need manual initialization, and the final results typically call for manual correction, specially when images are noisy.

Deep learning techniques have emerged as an alternative to circumvent these difficulties, when provided with enough annotated data. Their feasibility has been first demonstrated by Phellan *et al.* (2017), who proposed a 3D patch-based convolutional neural network (CNN) using pixel-wise annotations from two different anatomical planes. Kandil *et al.* (2018) proposed a similar architecture (Kamnitsas *et al.*, 2017) to exploit the intensity variations introduced by the changes in the blood flow. Aside from the pixel-wise annotations, the framework requires to split the brain into two sections: above and below the Circle of Willis. The global channel attention network (GCA-Net) (Ni *et al.*, 2020) captures multi-scale features through network branches specialized on learning feature information at different levels using 2D pixel-wise annotated image slices as input. To mitigate the limitations of neural nets in the segmentation of objects occupying small portions of an image, Livne *et al.* (2019) trained a Unet (Ronneberger *et al.*, 2015) on 2D pixel-wise annotated patches from a single anatomical plane. The 2D patches were randomly extracted from the original 3D volume, with half of the patches requiring to have a vessel in the center, thus requiring some further data pre-processing. Despite achieving accuracies similar to those of classical approaches, the main limitation towards the broader use of deep learning techniques remains to be the burden linked to pixel-wise data annotation, along with potential further pre-processing (e.g. (Kandil *et al.*, 2018; Livne *et al.*, 2019)).

Weak labels have been explored to address the limitations associated with data annotation. These include bounding boxes (Dai *et al.*, 2015; Rajchl *et al.*, 2017; Wang *et al.*, 2018), scribbles (Can *et al.*, 2018; Lin *et al.*, 2016; Wang *et al.*, 2015), con-

tours (Li *et al.*, 2018) and image tags (Ahn and Kwak, 2018; Hong *et al.*, 2017; Luo *et al.*, 2020), with the first three categories having been successfully used for weakly supervised segmentation of compact structures in medical images (Can *et al.*, 2018; Rajchl *et al.*, 2017; Wang *et al.*, 2018, 2015). In the context of general vessel segmentation, bounding boxes have been used for aortic segmentation (Pepe *et al.*, 2020). The aorta, however, is a rather compact structure that can be enclosed within a region of interest. This is not the case for highly sparse bifurcated trees, as the brain vascular tree, where a bounding box enclosing it would nearly cover the full brain. Similarly, scribbles and contours assume that the object to segment appears as a rather compact structure in a 2D image slice, where a single scribble or contour identifies it. This is not the case for 3D vessel trees. In a 2D slice, they appear as numerous disconnected blobs or elongated structures, making the use of scribbles or contours challenging. As a way to circumvent this, Koziński *et al.* (Koziński *et al.*, 2020) proposed to use 2D annotations in Maximum Intensity Projections (MIPs) of 3D vascular images. To some extent, these can be considered 2D image scribbles of varying density for the original 3D volume. The framework, however, requires full 2D pixel-wise annotations. Although the scheme significantly reduces the labeling time, more than four hours are needed to generate sufficiently dense 2D annotations that do not compromise the network’s performance.

As (Koziński *et al.*, 2020; Livne *et al.*, 2019), our aim is to address the current limitations of deep learning techniques for 3D brain vessel segmentation. Similarly to (Livne *et al.*, 2019), our framework builds upon the advantages of 2D patch-based approaches, making vessels cover a significant portion of the patch. To ease the burden of pixel-level labeling, we propose to use weak annotations in the form of image tags (Ahn and Kwak, 2018; Hong *et al.*, 2017; Luo *et al.*, 2020; Schlegl *et al.*, 2015). Differently from standard image tag-based methods, the proposed annotation scheme requires patch-level tags rather than image-level ones to cope with the granularity of vessels. To the best of our knowledge, image tags are most commonly used in

detection and classification tasks (Cheplygina *et al.*, 2019), but not as weak annotations to address medical image segmentation. .

The use of image tags for weakly supervised segmentation requires to generate pixel-wise labels using the user-provided tags as input. Similarly to previous works (Ahn and Kwak, 2018; Luo *et al.*, 2020), we generate the pixel-wise labels in a self-supervised fashion. The resulting set is used as the training data of a 2D network. Differently from previous works, we do not limit patch tags to the generation of pixel-wise labels. Instead, we propose to use them to train a classifier network for data augmentation. Under a multi-stage approach, the classification network discriminates unseen patches that can be subsequently used to synthesize pixel-wise labeled data for training of the segmentation network. This allows for a further reduction of the users annotation effort.

Most biomedical classification tasks rely on customized versions of VGG-16 (Simonyan and Zisserman, 2015) and ResNet (He *et al.*, 2016), the most popular architectures for natural image classification, or on task-specific architectures adapted from general purpose networks, such as stacked auto-encoders (Cheng *et al.*, 24454 2016) and end-to-end CNNs (Setio *et al.*, 2016), with no major performance differences currently found among them (Lundervold and Lundervold, 2019). We investigate the use of networks originally conceived for medical imaging tasks, i.e. the Unet (Ronneberger *et al.*, 2015) and the Pnet (Wang *et al.*, 2019), for the classification step of our framework. As these two networks were originally designed for image segmentation, we propose a way to adapt them to classification.

1.2. Contributions

The contributions of this work are four-fold:

1. we introduce an annotation and segmentation scheme, the Vessel-CAPTCHA, to reduce the labeling burden of 3D brain vascular images, consisting of two phases: a first phase where the user provides tags at the 2D image patch-level, and a second stage where pixel-wise labels are synthesized, in a self-supervised fashion, using only the user-provided patch tags as input.

2. We propose a weakly supervised learning framework on 2D image patches to achieve 3D brain vessel segmentation. To circumvent the problems faced by deep neural networks when segmenting small objects, the framework uses a 2D patch-based segmentation network trained with 2D weak pixel-wise labeled patches synthesized by the Vessel-CAPTCHA annotation scheme. To synthesize the weak labels, the Vessel-CAPTCHA only needs user-provided patch tags.
3. We investigate the use of network architectures specifically designed for medical imaging tasks to classify 2D image patches (vessel vs. non-vessel). The classifier network is used to enlarge the training set without further user effort and it acts as a filter in noisy segmentations.
4. Using two different image modalities, we demonstrate that the proposed framework achieves state-of-the-art performance for 3D brain vessel segmentation, while significantly reducing the annotation burden by ~80% compared to the annotation time required in other deep learning-based methods.

To foster reproducibility and encourage other researchers to build upon our results, the source code of our framework made publicly available on a Github repository¹.

2. Method

The proposed Vessel-CAPTCHA framework algorithm for 3D vessel segmentation is depicted in Fig. 1. In the following, we introduce the Vessel-CAPTCHA annotation scheme and we describe how weak pixel-wise labels are synthesized from the user-provided patch labels in a self-supervised way (Sec. 2.1). In Sec. 2.2, we present the two networks conforming the proposed framework: a classifier network and a segmentation network. Sec. 2.3 explains how the classifier network can be used to enlarge the set of weak pixel-wise annotations, allowing to have a larger set to train 2D-WnetSeg. Finally, Sec. 2.4 briefly explains how to segment unseen images using the proposed framework.

2.1. The Vessel-CAPTCHA Annotation Scheme

We consider a dataset \mathcal{I} of training images. Given an image $\mathbf{I} \in \mathcal{I}$ of size $H \times W \times S$, for each slice X_s , $s \in [1, \dots, S]$, we consider a partition in P_s non-overlapping patches: $X_s = \{\hat{X}_k\}_{k=1}^{P_s}$. Each patch is here considered as a function $\hat{X}_k : D_k \rightarrow \mathbb{R}$, where D_k is a subset of the slice domain $D_k \subset [1, H] \times [1, W]$.

User annotations on a given patch \hat{X}_k are defined through a function $U_k : D_k \rightarrow \{0, 1\}$, assigning a binary label to each coordinate $(i, j) \in D_k$. The set of annotations for a given patch is summarized by an indicator function $f : U_k \rightarrow \{0, 1\}$ which takes value 1 if at least one pixel in the patch was labeled with 1:

$$f(U_k) = 1 \iff \exists (i, j) \in D_k \text{ s.t. } U_k(i, j) = 1. \quad (1)$$

Fig. 2 illustrates examples of equivalent annotations. The set of indicators for the slice X_s is denoted by $\mathcal{Y}_s = \{f(U_k)\}_{k=1}^{P_s}$. The training set of patch-level labels for the image \mathbf{I} is defined by the set: $\mathcal{T}_P^{\mathbf{I}} = \{X_s, \mathcal{Y}_s\}_{s=1}^S$. This set is therefore composed by patches and associated indicators/tags of the presence of a vessel according to the user's annotation. Based on the training set $\mathcal{T}_P^{\mathbf{I}}$, we estimate approximated vessel masks via a model fitting procedure. For every patch we define a function $M_k : D_k \rightarrow \{0, 1\}$, which assigns to each pixel's coordinate a label according to the following scheme:

$$M_k(i, j) = \begin{cases} 0 & \text{if } f(U_k) = 0, \\ KM(\hat{X}_k(i, j)) & \text{otherwise,} \end{cases} \quad (2)$$

where KM is a K-means predictor trained on the intensity values of the patch $\{\hat{X}_k(i, j), (i, j) \in D_k\}$. By specifying $K = 2$ clusters we therefore obtain a rough estimate of the low-high intensity partitioning of the patch. The ensemble of estimated partitions across patches is denoted as $\mathcal{M}_s = \{M_k\}_{k=1}^{P_s}$, and we define the pixel-wise labeled training set for the image \mathbf{I} as $\mathcal{T}_M^{\mathbf{I}} = \{X_s, \mathcal{M}_s\}_{s=1}^S$.

Finally, patch- and pixel-level training sets across the image dataset are denoted by

$$\mathcal{T}_P = \{\mathcal{T}_P^{\mathbf{I}}\}_{\mathbf{I} \in \mathcal{I}}, \quad (3)$$

and

$$\mathcal{T}_M = \{\mathcal{T}_M^{\mathbf{I}}\}_{\mathbf{I} \in \mathcal{I}}, \quad (4)$$

¹<https://github.com/robustml-eurecom/Vessel-Captcha>

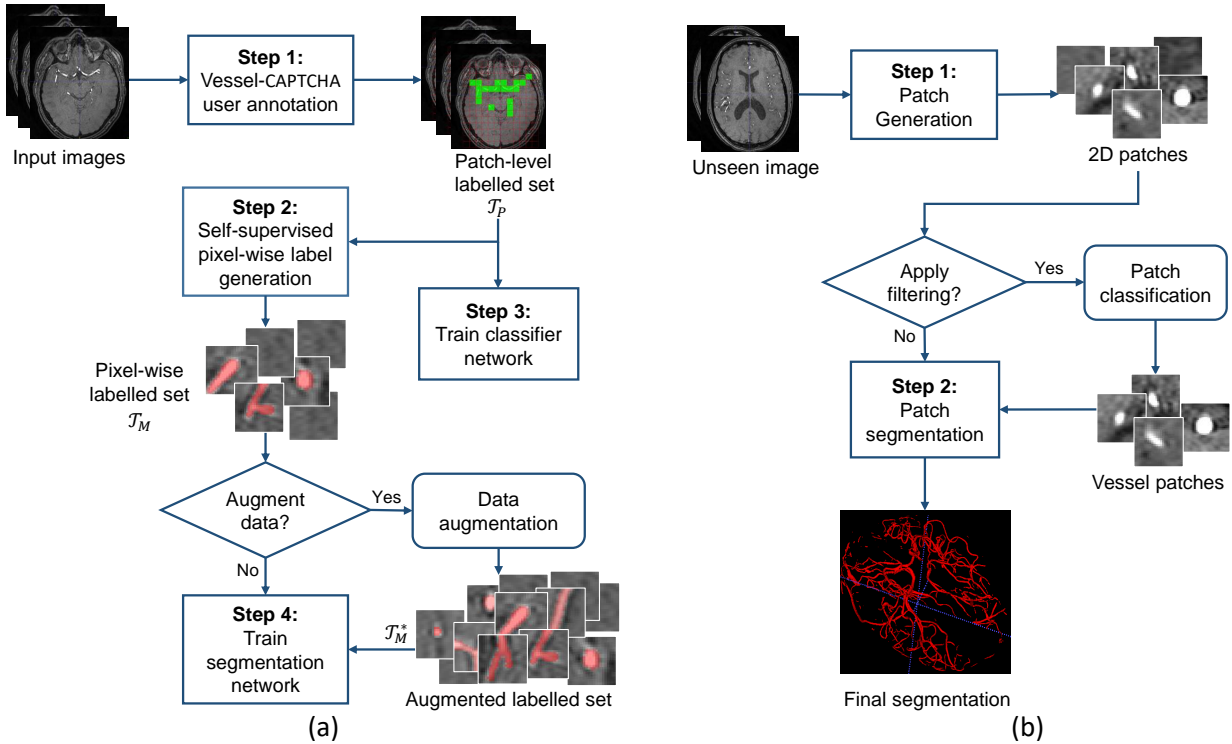


Fig. 1. Overview of the proposed Vessel-CAPTCHA framework algorithm. (a) Training phase: At step 1, user annotations are obtained through the Vessel-CAPTCHA and used to obtain pixel-wise labels in step 2. These two steps represent the Vessel-CAPTCHA annotation scheme. The provided user tags are also used in step 3 to train a classification network that can synthesize new weakly labeled data. To train the segmentation network (step 4) it is possible to enlarge the set of weakly annotated data through an optional data augmentation step. (b) Inference phase: For an unseen image, 2D patches are first obtained (step 1). In low quality images, where segmentations can be noisy, it is possible to use the classification network as a filter. In that case, only 2D segmentations from patches classified as containing vessels are considered for segmentation. At step 2, the segmentation network is used to perform patch-based segmentation. The final volumetric segmentation is obtained by concatenating the 2D segmentations. Rounded blocks denote optional steps.

respectively.

2.2. Patch Classification and Segmentation Networks

2.2.1. Networks for vessel vs. non-vessel patch classification

The classification network discriminates between vessel and non-vessel patches in unseen data. This discrimination serves two purposes: 1) to synthesize patch tags without the need of user interventions and 2) to act as a rough filter in noisy segmentations. The network is trained on \mathcal{T}_p .

Most works in the literature rely on customized versions of VGG-16 (Simonyan and Zisserman, 2015) and ResNet (He et al., 2016), the most popular architectures for natural image classification, or on task-specific architectures adapted from general purpose networks (Chen et al., 2016; Setio et al., 2016). In this work, we investigate the use of networks specifically designed for medical imaging applications for our classification task: the Unet (Ronneberger et al., 2015) and the Pnet (Wang et al., 2019). As these two networks have been designed for

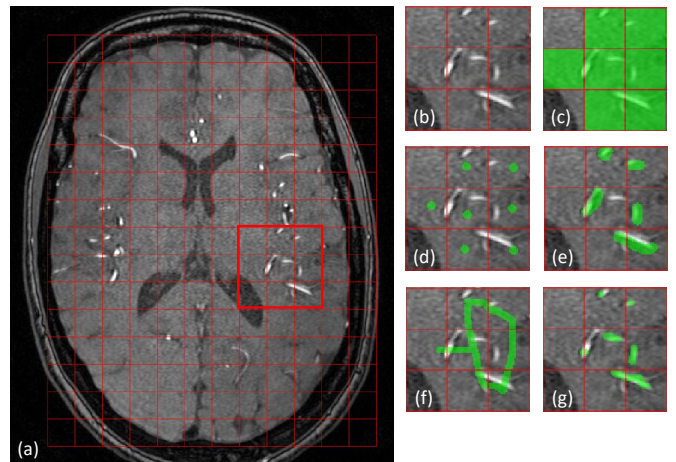


Fig. 2. Example of equivalent CAPTCHA annotations. (a) Image slice \mathcal{X}_s with patch grid, (b) zoomed region corresponding to the highlighted red box in (a), (c) resulting \mathcal{T}_p obtained through equivalent annotations (d-g).

image segmentation, we hereby describe how they have been modified to achieve classification.

We denote the modified 2D Pnet architecture (Wang et al., 2019) 2D-PnetCl. It consists of 7 convolution layers, 2 dropout layers, and a sigmoid layer. The first 5 convolution layers are concatenated. Each convolutional layer contains 64 filters with 3×3 voxels receptive fields in a 1 voxel stride sliding with different dilation factors. The dilations are 1, 2, 4, 8 and 16, respectively. The last two convolutional layers are the 1×1 convolutions, the output feature map is flattened and fed to a fully connected layer for interpretation with 128 hidden units and the final prediction layer uses a sigmoid function with one unit to classify patches with and without vessels. The adapted 2D-Unet architecture, denoted 2D-UnetCl, uses the network from (Livne et al., 2019) as a starting point. Similarly to the 2D-PnetCl, the output feature map is flattened and fed to a fully connected layer for interpretation with 128 hidden units and a final prediction layer with one unit to classify patches with and without vessels.

2.2.2. Segmentation Network

We use a segmentation network connecting two 2D-Unets in cascade (Dias et al., 2019). We denote it 2D-WnetSeg (Fig. 3). The network is trained on \mathcal{T}_M , the set of 2D image patches with weak synthesized pixel-wise labels to tackle the neural networks limitations in the segmentation of objects with a small object-to-image ratio.

The human cerebrovascular system has an intricate shape with large and smaller blood vessels which mainly differ in the spatial scale, but which share similar shapes. The selected self-supervised method, the K-means, favors the over-segmentation of larger vessels. Thanks to a set of max pooling layers, the first 2D-Unet allows to learn spatial scaling features from the input training data. Thus, it can recover rough-mask labels from smaller vessels not initially extracted by K-means. This means that the first Unet acts as a refinement module to correct the initial masks by inferring missing vessels based on the structural redundancy of the cerebrovascular tree. The second Unet, which has a similar architecture as the first one, receives as in-

put the output of the first Unet with the recovered labels from small vessels. As a result, the 2D-WnetSeg is able to learn vessels even with a weakly labeled training set with imperfect labels or noise.

The smaller vessels in the brain vessel tree may disappear in very deep networks due to the subsampling layers. To tackle this, the 2D-WnetSeg has 14 blocks with convolutional layers structured into 4 levels. In this, it differs from previously proposed cascaded networks (Dias et al., 2019) or the Unet-based vessel segmentation from (Livne et al., 2019). This also contributes to reduce the number of trainable parameters. Specifically, the number of trainable parameters in (Livne et al., 2019) is about $3.1e7$, whereas the WnetSeg has only about $1.6e7$ parameters.

In our architecture, the first 7 blocks form the first Unet and the second 7 blocks belong to the second one. Each block consists of 2 convolutional layers with kernel size 3×3 pixels, each followed by a rectified linear unit (ReLU). They are both added to the padding to ensure that the output has the same shape as the input. A drop-out layer is applied between them. As the input proceeds through different levels along the contracting path, its resolution is reduced by half. This is performed through a 2×2 max-pooling operation with stride 2 on 3 levels except for the bottom level. We double the number of feature channels at each level of the contracting path. The right portion of a half-network (Unet), i.e. the expansive path, consists of blocks with concatenation and up-sampling for each level to extract low-features and it expands the spatial support of the lower resolution feature maps to assemble the necessary information and recover the original input size. Finally, we employ skip-connections from the shallow layers to deeper layers between the two 2D-Unets, at the same levels, to ease the training of the network.

2.3. Data Augmentation for Segmentation Network Training

The set \mathcal{T}_M consisting of weak annotations is used to train the 2D-WnetSeg. To augment its size without increasing the annotation burden, we make use of the classification network to generate a larger set of weak annotations. The procedure is

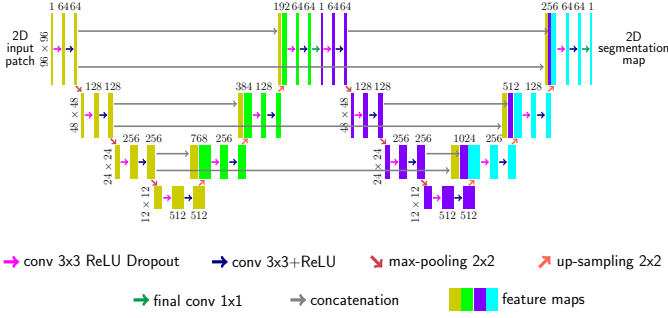


Fig. 3. Illustration of the 2D-WnetSeg architecture.

depicted in Fig. 4.

Assuming that there is an initial set of unlabeled images I^* that can be used for training, we consider the joint image dataset of labeled and unlabeled images $I_{ALL} = I \cup I^*$. The subset I of these images is used to generate Vessel-CAPTCHAs, which are presented to the user for annotation. This results in the training set \mathcal{T}_P (Eq. 3), which is used to both train the classification network and to synthesize the weakly pixel-wise labeled set \mathcal{T}_M (Eq. 4).

Using the trained classification network, a set of patches $\{\mathcal{X}_s^*\}$ is obtained in the remaining set of images I^* . Rather than presenting another Vessel-CAPTCHA to the user for annotation, the $\{\mathcal{X}_s^*\}$ are inputted to the classification network to estimate patch labels $\{\mathcal{Y}_s^*\}$. The paired set of patches and estimated labels conform a new set $\mathcal{T}_P^* = \{\mathcal{T}_P^1\}_{I \in I^*}$.

The set \mathcal{T}_P^* is used to synthesize weak pixel-wise label masks M^* following the same procedure applied to \mathcal{T}_P (Sec. 2.1). This leads to a new weakly labeled set \mathcal{T}_M^* . The extended set of weak pixel-wise labels is formed by the union of the two sets $\mathcal{T}_{M_{ALL}} = \mathcal{T}_M \cup \mathcal{T}_M^*$, and is subsequently used to train the 2D-WnetSeg architecture.

2.4. Inference Phase

Unseen 3D images are segmented by extracting 2D image patches that are then segmented by the 2D-WnetSeg and concatenated to build back the original volume (Fig. 1(b)). In noisy images, it is often the case that the resulting segmentation can present a large set of pixels erroneously segmented as vessels. To avoid this problem, the trained classifier network can act as a filter in the segmentation pipeline. In such case, only those

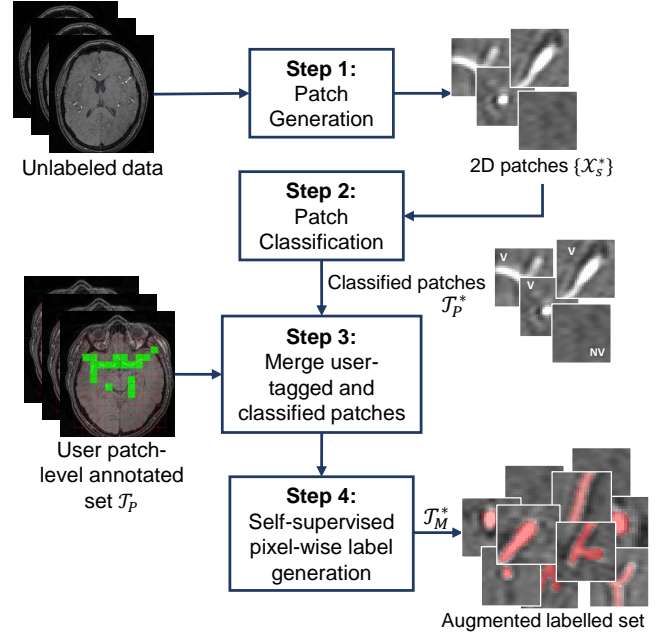


Fig. 4. Data Augmentation procedure. The trained classifier is used as the starting point to enlarge the initial pixel-wise labeled training set \mathcal{T}_M without requiring further user inputs. The resulting training set $\mathcal{T}_{M_{ALL}}$ is a combination of both the synthesized labels and those obtained via the Vessel-CAPTCHA annotation.

patches which have been classified as vessels are taken into account to reconstruct the final volume. All the pixels of the remaining patches are set to zero.

2.5. Implementation Details

We used the Keras library to implement 2D-PnetCl, 2D-UnetCl and 2D-WnetSeg. The networks were trained on a GPU workstation with 4-core Intel(R) Xeon(R) CPU @ 2.30GHz, a NVIDIA Tesla P100-PCIE-16GB, and 25GB memory. For both 2D-UnetCl and 2D-PnetCl we optimized the binary cross-entropy loss function with a minibatch stochastic gradient descent and a conservative learning rate of 0.01 and momentum of 0.9. For 2D-WnetSet, we used an objective function based on the Dice score coefficient, as proposed by Milletari et al. (2016), which is specifically tailored for segmentation tasks in medical images. The weights of this model were optimized using an Adam optimizer with learning rate $lr = 1e-4$, $\beta_1 = 0.9$, and $\beta_2 = 0.999$. All networks were trained from scratch using mini-batches of 64 patches. All input patches were normalized by the mean and standard deviation of the whole training data. A dropout of 0.5 for PnetCl and UnetCl, and of 0.1 for

WnetSeg was added to prevent overfitting during the training.

3. Experiments and Results

In this section, we first introduce the experimental setup. Then we present experiments to assess the role of the weak labels in the framework’s performance followed by a comparison of the studied classification networks. Next, we perform an ablation study to understand how the different components of the framework contribute to performance. We then compare our framework to different state-of-the-art methods in terms of both performance and annotation time using Time-of-Flight (TOF) angiography images and perform a conclude the section with a qualitative evaluation of results on Susceptibility-Weighted Images (SWI).

3.1. Experimental Setup

3.1.1. Data

Two different magnetic resonance imaging sequences were used for evaluation: Time-of-Flight (TOF) angiography and SWI. Both modalities are commonly used to image and assess the cerebrovascular tree (Radbruch *et al.*, 2013). Blood vessels present different appearances in each of these modalities. In TOF, vessels are hyper-intense structures, whereas they are hypo-intense in SWI.

Forty-two TOF subject scans were available with volume dimensions $560 \times 560 \times 117$ and isotropic voxel size $1 \times 1 \times 1 \text{ mm}^3$. For SWI, we used 30 different subject scans with image dimensions $480 \times 480 \times 288$ and isotropic image resolution $1 \times 1 \times 1 \text{ mm}^3$. Due to poor image quality, three SWI scans were discarded for the experiments. We performed data splitting at the subject-scan level, using images from 25, 7, 10 and 15, 5, 7 patients for training, validation and testing in TOF and SWI, respectively. The training and validation sets were annotated using the Vessel-CAPTCHA. The training set consisted of 517.5K and 24.3K 2D patches (size 32×32) for TOF and SWI, respectively. The validation set consisted of 144.9K and 8.1K 2D patches (size 32×32) for TOF and SWI, respectively. The training sets were augmented through the use of different random rotations, flips and shears at every epoch for every 2D patch.

3.1.2. Setup and Evaluation Metrics

An experienced rater used the Vessel-CAPTCHA annotation scheme to label all the available images, using patches of size 32×32 . Before generating the Vessel-CAPTCHA, all images were skull-stripped using a standard tool. As a result, the annotation grid is generated only around the brain tissue (see Fig.2).

Two different rules were used to synthesize the weakly annotated training sets \mathcal{T}_M with the K-means algorithm. In TOF, vessels were associated to the cluster with the highest mean value, whereas the vessel class was associated to the cluster with the lowest mean value in SWI. The training sets, \mathcal{T}_P and \mathcal{T}_M , were used to separately train models, i.e. a classification and a segmentation network per modality.

To assess the quality of the classification results obtained by 2D PnetCl, we measured precision (P), recall (R) and the F-score (F_1)

$$P = \frac{TP}{TP + FP}, \quad R = \frac{TP}{TP + FN}, \quad F_1 = 2 \frac{P \cdot R}{P + R} \quad (5)$$

where a true positive, TP , represents a patch correctly classified as vessel. False positives FP s and false negatives FN s are non-vessel patches classified as vessels and vice versa. We compared the 2D-PnetCl and 2D-UnetCl with VGG-16 (Simonyan and Zisserman, 2015) and ResNet (He *et al.*, 2016), as they are two of the most common networks for classification.

For TOF, the testing set was pixel-wise annotated by the expert rater. The Dice Score Coefficient (DSC) between the segmentation and the annotated ground truth was used for a quantitative assessment:

$$DSC = \frac{2|S \cap \mathcal{G}|}{S + \mathcal{G}}, \quad (6)$$

where S and \mathcal{G} represent the set of pixels segmented by the proposed method and the manual annotations of the same image, respectively. For SWI, since it is difficult to obtain a sufficiently robust ground truth, the segmentations were qualitatively assessed through visual inspection by an expert rater and classified as good, average or poor quality.

Vessel-CAPTCHA was compared with different networks: the deep learning-based brain vessel segmentation framework from

Livne et al. (2019) (Vessel 2D-Unet), which relies on the 2D-Unet (Ronneberger et al., 2015) as backbone architecture, the 2D Pnet (Wang et al., 2019), and the 3D-Unet (Çiçek et al., 2016). These networks require pixel-wise annotations, so the TOF training set was fully annotated. For the Vessel 2D-Unet, further data pre-processing was performed as described in (Livne et al., 2019).

In addition to deep learning approaches, we compared the proposed Vessel-CAPTCHA with three traditional non-learning based approaches. These are: the Frangi filter (Frangi et al., 1998) and the Sato filter (Sato et al., 1997), which are a reference for vessel segmentation, and a tensor voting framework for brain vessel segmentation (Zuluaga et al., 2014b).

3.2. Self-Supervised Pixel-wise Labels Generation

We study how the weak pixel-wise labeled dataset \mathcal{T}_M synthesized from user-provided patch tags affects the framework’s performance in TOF. We achieve this in two ways. First, we investigate if the weak pixel-wise labels synthesized by K-means represent a good rough approximation of pixel-wise user-annotated labels. Second, we assess how the size of the patches used as input of the segmentation network influences the latter’s performance. In our experiments, we compare with Gaussian mixture models (GMM), an alternative self-supervised approach that allows to obtain weak pixel-wise labels. Two components (vessel and background) are used for the GMM to be comparable with K-means. For both cases, patches with more than 30% pixels marked as vessel were fully masked out and considered as non-vessel. These correspond to highly noisy patches containing only brain tissue.

The role of the self-supervised method, i.e. the K-means in our case, is to synthesize pixel-wise label masks $\{\mathcal{M}_s\}_{s=1}^S$ which are sufficiently good to train the segmentation network. In other words, the synthesized weak labels should be as close as possible to hypothetically pixel-wise annotations provided by a user. We thus measure the similarity between the synthesized pixel-wise label masks $\{\mathcal{M}_s\}_{s=1}^S$ and the available pixel-wise annotations of the TOF training set. The K-means (and GMM) are applied on different input sizes, namely directly on the full im-

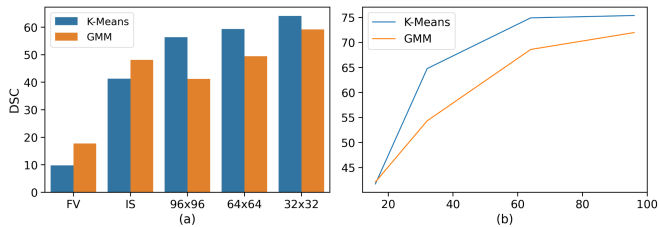


Fig. 5. (a) Similarity between user-provided pixel-wise annotations and weak pixel-wise labels obtained through K-means and GMM, measured through the DSC in TOF. K-means and GMM are applied on the full volume (FV), on a per slice basis (IS) and on different patch sizes. (b) 2D-WnetSeg performance using synthesized weak pixel-wise labels by K-means and GMM for different input patch sizes (16, 32, 64 and 96).

age volume, or on subsets of it that are then concatenated. For this we use image slices and patches of varying sizes: 96, 64 and 32. For the patches, K-means and GMM are only applied to vessel patches. We set 32 as the smallest patch size, which corresponds to the size set for the Vessel-CAPTCHA, i.e. the user-input. Larger patches were obtained by concatenating the user input into a 2×2 and 3×3 grid.

Fig. 5(a) shows the similarity between the training set pixel-wise annotations and the weak pixel-wise label masks measured in terms of the DSC. The performance of both methods is inverse to the size of the input sample. As it would be expected, when applied to large extents of the image volume, i.e. the full image volume (FV) or on a per image slice basis (IS), the DSC is very low ($< 40\%$), with GMM reporting slightly higher values. As the extent of the input sample decreases, i.e. using patches, K-means performs better, which could be justified by the fact that smaller regions tend to be more homogeneous. Two aspects should be highlighted from the obtained results. Firstly, we observe that GMMs lead to thinner vessel masks than those synthesized by K-means (Fig. 6), which is consistent with the higher DSC, as over-segmentations tend to be less penalized than mis-segmentations. Given the way that the 2D-WnetSeg learns, it is better to have overestimated masks from K-means than the finer ones. However, being K-means a simpler algorithm, the patch size used as the input plays an important role. Our results suggest that smaller patch sizes lead to better results. Secondly, we shall recall that both self-supervised methods are only applied to vessel patches. This is a necessary condition

to obtain weak labels of a minimum quality using these two algorithms. The condition is guaranteed by the patch tags discriminating vessel from non-vessel patches, which are obtained through the Vessel-CAPTCHA. Based on these results, for the remaining experiments we set the patch size input to the K-means to 32×32 , which corresponds to the same value used in the Vessel-CAPTCHA.

Fig. 5(b) shows the 2D-WnetSeg accuracy with varying input patch sizes over the validation set. The patches are obtained by rebuilding the rough mask volume from the 32×32 patches and re-cropping the volume into different patch sizes. It should be noted that the segmentation network’s input patch size does not have to match that one of the Vessel-CAPTCHA. Coherently with the previous results that show that K-means synthesized labels that are more similar to true annotations, their use consistently leads to higher DSCs. The Vessel-CAPTCHA patch size, 32×32 , seems too small for the 2D-WnetSeg to capture the features that allow to discriminate vessel pixels from non-vessel ones. Instead, larger patches lead to higher DSCs. However, we avoid the use of larger patch sizes to avoid the problem of vessels becoming a small portion of the full image/patch, leading to drops in performance. We set the segmentation network’s input patch size to 96×96 in our remaining experiments. By enlarging the size of the patch, the training and validation sets were resized to 57.5K and 16.1K, respectively, for TOF.

3.3. Classification network

We study the performance of the two classification networks, 2D-UnetCl and 2D-PnetCl, to determine if they are well-suited as discriminators within our framework. Table 1 compares the classification performance of 2D-UnetCl and 2D-PnetCl in TOF and SWI images with VGG-16 and the ResNet. For each network, two models were trained, one for TOF and one for SWI, using the annotated training data \mathcal{T}_P obtained with the Vessel-CAPTCHA (see Sec. 3.1.1). Results are reported on the best performing model in the validation set.

The two proposed networks, derived from medical imaging task-specific networks, present a higher overall performance (F-score) than VGG-16 and the ResNet. This suggests that the

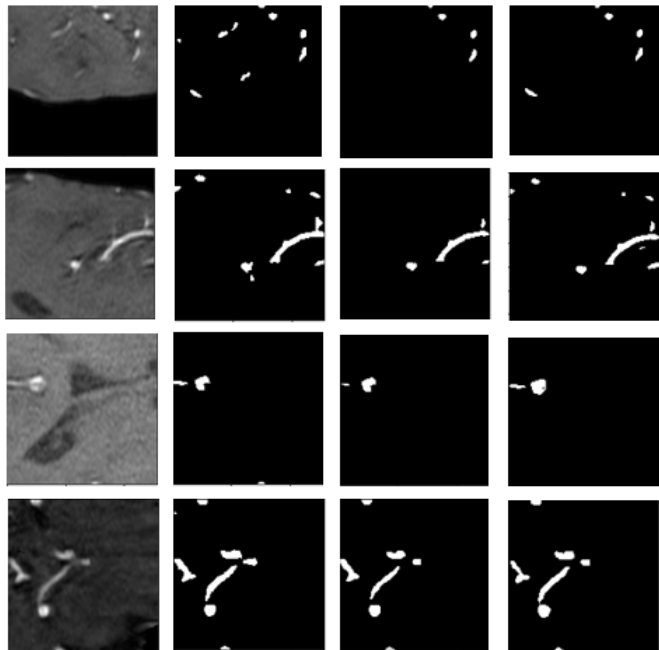


Fig. 6. Examples of the generated training set \mathcal{T}_M . From left to right original TOF image, ground truth, GMM synthesized labels and K-means synthesized labels.

use of networks specifically designed for medical imaging tasks does contribute to an increased performance. All methods report a drop in performance from TOF to SWI, which is expected given that SWIs are more challenging to classify and segment due to several factors. First, vessels in SWI are hypo-intense, being similar in appearance to the image background. As such, vessels close to the brain surface are prone to misclassification. Second, SWI is capable of imaging very small vessels that can be difficult to identify within a patch, as they can have an appearance similar to the one of brain tissue inhomogeneities or sulci, this leading to misclassification.

When comparing the two proposed networks, 2D-PnetCl presents in both image modalities the highest performance when considering both vessel and non-vessel patch classification. This reflects a good balance in the network’s capability to discriminate among vessel and non-vessel patches, which is key for its use within the Vessel-CAPTCHA framework. In the remaining of the paper, we rely only on 2D-PnetCl as a classification network.

Table 1. Classification network comparison in TOF and SWI. For each row, bold font denotes the best value, with underlined values not significantly different from it ($\alpha = 0.05$)

		VGG-16	ResNet	2D-UnetCI	2D-PnetCI
TOF	Precision	92.48±1.54	93.66±1.48	<u>94.82±0.48</u>	94.91±1.04
	Recall	87.39±4.60	93.27±1.73	<u>94.04±0.65</u>	94.94±1.09
	F-score	88.68±3.81	93.34±1.62	<u>94.27±0.54</u>	94.71±1.23
SWI	Precision	<u>82.34±1.15</u>	80.14±1.13	<u>82.44±1.18</u>	82.97±1.55
	Recall	77.45±4.17	79.39±3.35	74.35±5.35	<u>79.30±4.07</u>
	F-score	78.76±3.39	<u>79.17±2.31</u>	76.42±4.63	80.31±3.31

Table 2. 2D-WnetSeg vs single Unet performance (DSC) for varying training set sizes $|\mathcal{T}_M|+|\mathcal{T}_M^*$ in TOF. Bold font denotes the best value with significant improvement (p -value < 0.05) per row, and (*) the best value overall

$ \mathcal{T}_M + \mathcal{T}_M^*$	2D-WnetSeg	One 2D-Unet
15+0	75.96±3.07	73.53±4.45
15+10	*76.35±2.29	71.78±2.00
25+0	76.30±2.74	74.39±2.22

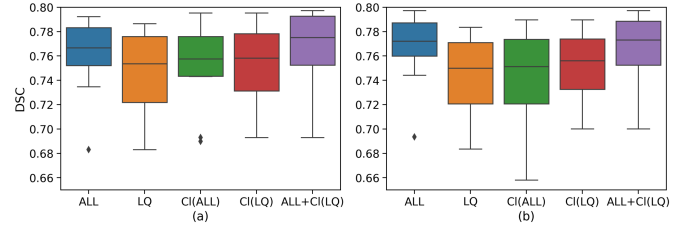


Fig. 7. Classification network as a noise filter in TOF. Vessel segmentation DSC for all the test set (ALL), low quality test images (LQ), full test set filtered (CI(ALL)), low quality images filtered (CI(LQ)) and full test with only the low quality filtered (ALL+CI(LQ)) using WnetSeg trained on (a) the original training set and (b) augmented training set.

3.4. Ablation Study

We study the properties of the different components of the proposed annotation and segmentation framework through a set of ablation studies. We investigate the role of the 2D-WnetSeg network, and the use of the classification network for data augmentation and as a noise filter.

3.4.1. Segmentation Network

Table 2 compares the final output of 2D-WnetSeg with the output of its first Unet (2D-Unet). The 2D-WnetSeg reports a higher DSC. The better performance of the 2D-WnetSeg is explained by the fact that the deep networks are trained on rough segmentation maps. The first Unet works as a refinement module to correct the mask by inferring potentially missing vessels based on the structural redundancy of the cerebrovascular tree. The second Unet can learn from the raw brain image and the previously improved segmentation mask, leading to an increase of the segmentation performance. The single Unet, instead, is faced directly with the rough masks.

3.4.2. Data Augmentation

Table 2 presents the DSC of the 2D-WnetSeg in three different scenarios with varying size of the training set ($|\mathcal{T}_M|+|\mathcal{T}_M^*$): 1) A training set with the 15 patch-annotated images, no data augmentation (15+0), 2) a training set with 15 patch-labeled images and 10 images (15+10) automatically labeled through

the data augmentation process (Fig. 4), and 3) the full training set with user-provided patch-tags (25+0). The results show that the data augmentation step (15+10) improves performance w.r.t. using the same annotated training set with no augmentation (15+0), while reaching a comparable performance to that one of using a dataset entirely annotated by the user (25+0). The comparable performances (15+10 vs. 25+0) come as a result of the high classification accuracy of the 2D-PnetCI (F-score=94.71%), which sits close to the performance of a human rater. This close difference, however, seems to undermine the performance of the ablated WnetSeg, when the second Unet is removed. The potential errors incurred by the classifier network cannot be recovered by the single network, which confirms that 2D-WnetSeg is best suited for the proposed setup.

3.4.3. Noise Filter

Fig 7 reports vessel segmentation DSC in the following scenarios: 1) on all the testing set (ALL); 2) on 4 images identified as of low quality (LQ); 3) applying the noise filter to the all testing set (CI(ALL)); 4) applying the noise filter to the low quality data (CI(LQ)); and 5) in all the testing set with the noise filter applied only to low quality data (ALL+CI(LQ)). Results are re-

ported for the WnetSeg trained with the original weakly labeled dataset (15+0) and the augmented one (15+10).

The results show that filtering has a significant impact in the segmentations' accuracy and variability for low quality (LQ) images (p -value<0.05), although when applied to the full test set there is a slight drop in accuracy ($\sim 1.9\%$). This indicates that the filter has a negative impact on the segmentation accuracy of high quality images. As a result, one could consider a setup where images are inspected and the noise filter would be applied only to those identified as of low quality, which would lead to a higher overall performance. In such a setup, the WnetSeg trained with 15 images (Fig 7(a) ALL+Cl(LQ)) reaches testing accuracy very close to that one of the WnetSeg trained with augmented data. This suggests that the classification network used as a noise filter represents an alternative to improve accuracy without the need of further training data, but at the cost of requiring a visual inspection step.

3.5. Method Comparison

We benchmark the Vessel-CAPTCHA against different state-of-the-art networks and traditional vessel segmentation methods in terms of performance and training set annotation time. For every compared learning-based method, two models are trained with two training set sizes (15 and 25). The models are chosen on the best performance in the validation set. Table 3 summarizes the hyperparameter setup for every benchmark network. Regarding the traditional segmentation methods, the Frangi and Sato filters produce real-valued maps that need to be thresholded to get a binary segmentation. The tensor voting provides a probability map, but may produce small spurious segmentations that need to be filtered out. We obtain final binary segmentations for these methods in two ways. In one case, we do not do any post-processing (NP): the real-valued masks obtained with the Frangi and Sato filter are normalized to the range $[0, 1]$, we set a fixed threshold ($t > 0.6$) to binarize the three maps, and we do not filter out potential small spurious objects. In the second scenario, we post-process (PP) the maps. Here, every (real-valued and probability) map is inspected by overlaying it on the original testing image, to define and apply a per-image

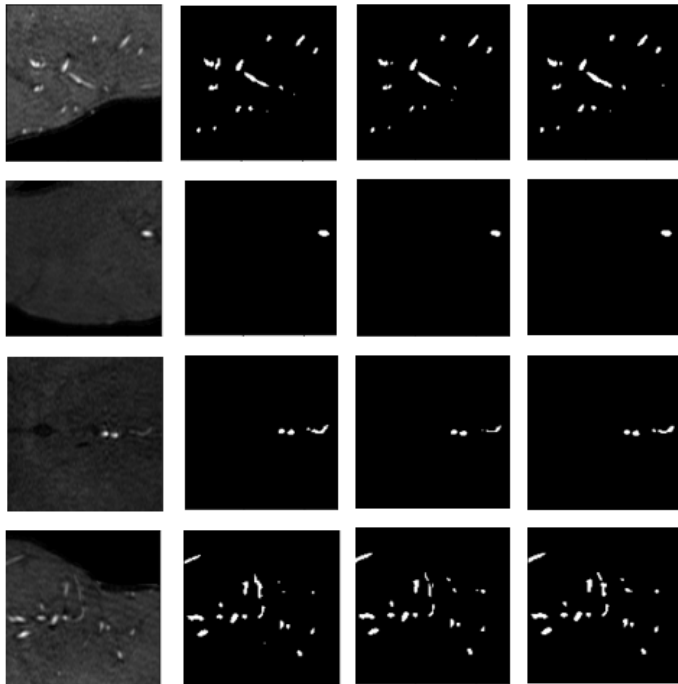


Fig. 8. Segmentation results in TOF images. From left to right: original image, ground truth, Vessel 2D-Unet and Vessel-CAPTCHA.

threshold. The resulting binary maps are filtered by masking out any connected component with a size equal or smaller than 4. Through visual inspection of every binary segmentation overlaid in the original image, the minimum connected component size could be modified.

Table 4 reports the DSC of the evaluated methods. We include results for the standard Vessel-CAPTCHA, with and without data augmentation, and noise filtering. Furthermore, we report results for the 2D-WnetSeg when trained on fully annotated data. The Vessel-CAPTCHA reports the best results using both data augmentation and noise filtering. As previously discussed, however, the noise filtering step requires visual inspection to select which images should be filtered. Nevertheless, our method remains the best performing without the filtering step. The results do not show statistical differences with the Vessel 2D-Unet (25) (Livne et al., 2019), which is considered the current state-of-the-art regarding learning-based methods for brain vessel segmentation. This demonstrates that the proposed framework can reach state-of-the-art performance despite the use of less accurate annotations (Fig. 8).

Interestingly, our segmentation network, the 2D-WnetSeg

Table 3. Hyper-parameter setup for compared networks

Network	Hyperparameters
Vessel 2D-Unet	batch size: 64, lr 1e-4, dropout: 0.0
2D-Pnet	batch size: 8, lr: 1e-4, dropout: 0.2
3D-Unet	lr: 1e-4, reduced by 0.5 every 10 epochs, max epochs: 500 epochs Stopped at 50 epochs if no improvements in the validation error

Table 4. Quantitative comparison with state-of-the-art methods in TOF. The bold font denotes best value, with underlined values not significantly different from it ($\alpha = 0.05$).

	Method ($ \mathcal{T}_M + \mathcal{T}_M^*$)	DSC (%)
No labels	Frangi Filter NP (0)	55.31±7.61
	Frangi Filter PP (0)	68.42±3.10
	Sato Filter NP (0)	57.57±6.14
	Sato Filter PP (0)	69.77±3.42
	Tensor Voting NP (0)	71.41±3.81
	Tensor Voting PP (0)	73.22±3.38
	Fully labeled	2D-Pnet (15)
2D-Pnet (25)		73.11±3.34
Vessel 2D-Unet (15)		75.05±2.91
Vessel 2D-Unet (25)		<u>75.59±2.99</u>
3D-Unet (15)		63.99±3.33
3D-Unet (25)		63.55±3.60
2D-WnetSeg (15)		73.12±3.57
2D-WnetSeg (25)		75.22±2.29
Weakly labeled	Vessel-CAPTCHA (15)	<u>75.96±3.02</u>
	Vessel-CAPTCHA (15)+Filter	<u>76.23±2.91</u>
	Vessel-CAPTCHA (15+10)	<u>76.35±2.97</u>
	Vessel-CAPTCHA (15+10)+Filter	76.53±2.89
	Vessel-CAPTCHA (25)	<u>76.30±2.74</u>

NP: No post-processing, PP: Post-processing

with pixel-wise annotated data has a lower performance than the Vessel 2D-Unet, which is coherent with the behavior observed in Sec 3.4.1. While the two-stage refinement procedure of the 2D-WnetSeg plays a role when trained with rough segmentation masks, where annotations are more refined the presence of the stacked Unet results detrimental to performance. 2D-WnetSeg requires slightly overestimated masks to compensate for information loss over the two-stage approach. The 2D Pnet reports slightly lower results; however, it significantly surpasses those of the 3D-Unet. The poor performance of the 3D-Unet explains why 3D networks are not used for brain vessel segmentation as they have a lower performance than traditional approaches. Finally, traditional non learning-based vessel segmentation methods show a poor performance when no manual post-processing is done. This is expected, as it is a well-known limitation of such approaches. The post-processing step allows an important

Table 5. Total average time needed to annotate one dataset using full pixel-wise annotations (TOF) and the Vessel-captcha annotation scheme (TOF and SWI). DSC is reported for TOF images

Method	Time (min)	DSC
2D-UNet TOF (25)	327	75.59±2.99
Vessel-CAPTCHA TOF (15+10)	68	76.35±3.29
Vessel-CAPTCHA SWI	94	-

jump in performance, but it requires high expertise and it is time consuming.

We record the time required to annotate all the dataset with the Vessel-CAPTCHA annotation scheme and to fully pixel-wise annotate TOF images used to train Vessel 2D-Unet, 2D Pnet and the 3D-Unet. Table 5 presents the results along with the best performance achieved for each method. We only report results for the Vessel 2D-Unet, as it is the best performing method from the benchmark, and all other networks share the same annotation time.

The Vessel-CAPTCHA reduces the annotation time by 79% w.r.t. pixel-wise annotations in the same image, while achieving a better accuracy. It is worth noting that the reported time for the full annotation only considers the labeling time. For instance, the Vessel 2D-Unet framework (Livne et al., 2019) requires additional data pre-processing to obtain patches with vessels located at the center of the patch, which is not considered in the reported numbers. This operation could represent a further increase in the time needed to prepare the training set.

Table 6 compares the evaluated networks in terms of model size, FLOPs and training time. The inference time was not included, as it takes less than a minute to segment an image for every network. This represents a significant difference w.r.t. the traditional approaches, which are particularly slow at inference. Using ten different scales for each of them, the Frangi and Sato filter take ~15 mins to segment an image, whereas the tensor voting method takes ~25 mins, without considering any post-

Table 6. Comparison of model complexity (Params, FLOPs) and training time in hours of the benchmarked networks. The Vessel-captcha reports values of the segmentation network

Model	Params (M)	FLOPs (G)	Training (h)
2D-Pnet	0.48	8.93	0.5
Vessel 2D-Unet	31.38	15.6	1.5
3D-Unet	16.21	1669.53	1.0
Vessel-CAPTCHA	16.34	25.90	1.5

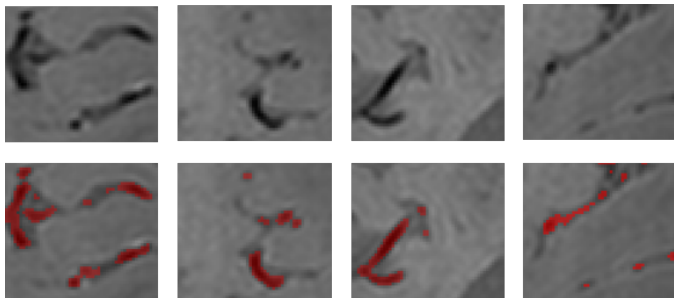


Fig. 9. Segmentation results in SWI images. Top: Original image. Bottom: Overlaid segmentation. From left to right the first three cases present good segmentation results. The rightmost example shows a sulci that has been segmented as if it was a vessel.

processing step. In terms of model complexity, our approach has model size (see Params), comparable to other assessed networks and a slightly higher number of FLOPs than the other 2D-networks.

3.6. SWI: Qualitative Evaluation and Annotation Time

We perform a qualitative assessment of the SWI vessel segmentations, as this dataset does not have pixel-wise annotated ground truth. The 2D-WnetSet was trained and visually assessed on the validation set. The model visually judged as best was used to segment the test set. Similarly to TOF, 2D 96×96 patches were used for the 2D-WnetSeg training. This represents 27K training samples.

Fig. 9 presents examples of the segmentations obtained in SWIs. Overall, this modality is more complex than TOF, thus further errors are observed. As a general pattern, the segmentations in SWI tend to miss small vessels, while there is also a high incidence of false positives due to erroneously segmented sulci and noise. Based on a visual inspection by an expert rater, the segmented images were classified as of good, average or low quality. A segmented image is considered good, if it segments the large and medium vessels, and avoids the segmentation of noisy regions, with an elongated appearance similar to a ves-

Table 7. Qualitative assessment of segmentation results in SWI with and without noise filtering. Segmentations are classified as good, average or low quality through visual assessment

	Good	Average	Low
Before filtering	2	3	2
After filtering	4	2	1

sel, and sulci. It might miss some small vessels. A segmented image is considered of average quality if it segments large and medium vessels, it misses small ones, it may segment noisy areas in a small proportion (less than 50%), specially in the anterior part of the brain, and often segments sulci. All other cases are considered as low quality ones.

Table 7 reports the qualitative assessment, using the visual judgment of the segmentation results with and without the noise filter. The use of the filter improves the quality of four segmentations, according to the visual assessment. As illustrated in Fig. 10, the classification filter allows to correct segmentations containing large regions of false positives caused by noise in the image, mostly in the boundaries of the brain tissue. As with TOF, its use might require a first visual inspection of the segmentation results to decide if it should be applied or not.

SWI Vessel-CAPTCHA annotation requires 38% more time than in TOF (Table 5). This is expected given the increased complexity of SWI scans: small vessels require more effort to be identified and vessels often present an appearance similar to sulci (Fig 9). These factors have a direct incidence in the time needed by a rater to discriminate vessel from non-vessel patches. Nevertheless, SWI Vessel-CAPTCHA accounts for 71% less time than the pixel-wise annotation baseline (Table 5).

4. Discussion and Conclusions

In the recent years, deep convolutional networks have achieved state-of-the-art performance in medical image segmentation tasks, but their success has not been as wide for 3D brain vessel segmentation. This can be explained by two factors. First, as it has been highlighted by previous works (Livne *et al.*, 2019), deep learning techniques are less performing when the object of interest occupies a small portion of the image. This is the case of brain vessels, where only 0.9% of brain voxels

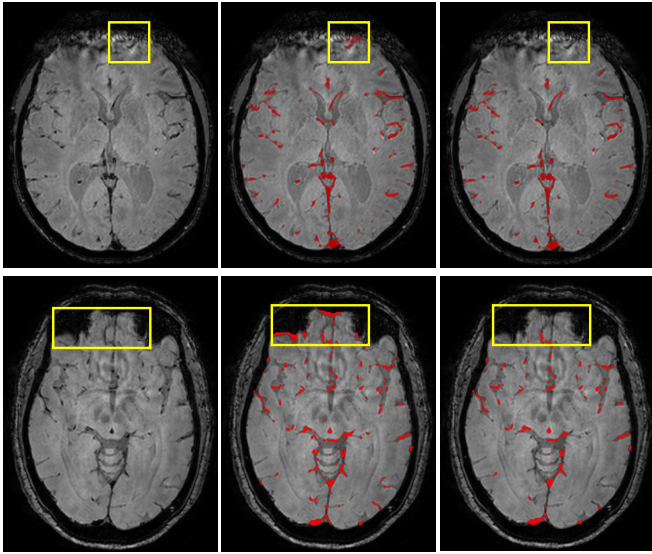


Fig. 10. Classification network as a noise filter in two SWI slices. From left to right, original image, segmentation from 2D-WnetSeg, segmentation after filtering. The yellow boxes highlight areas with image noise that are first segmented as vessel, but corrected with the filter.

within a slice are vessels (Livne *et al.*, 2019). Second, manual pixel-wise annotation is highly time consuming and complex (Moccia *et al.*, 2018). In this work, we have introduced the Vessel-CAPTCHA, an efficient learning framework for vessel annotation and segmentation to address the two above-mentioned limitations. The framework formulates the Vessel-CAPTCHA annotation scheme, which allows users to annotate a dataset through simple clicks on patches containing vessels, similarly to the commonly used image-CAPTCHAs of web applications (von Ahn and Dabbish, 2004). To the best of our knowledge, this is the first work that relies only on image/patch tags as input for learning-based medical image segmentation (Cheplygina *et al.*, 2019). Similar to previous works on weakly supervised image segmentation using image tags (Ahn and Kwak, 2018; Luo *et al.*, 2020), the obtained patch-level tags are used to synthesize weak pixel-wise labels in a self-supervised fashion. The resulting weak pixel-wise labeled dataset is used to train a 2D patch-based segmentation network, which performs the final segmentation. In our work, we have chosen to use the K-means algorithm to synthesize the weak pixel-wise labels along with the proposed 2D-WnetSeg network, concatenating two 2D-Unets, as backbone architecture. Our results show that the complementary characteristics of the two allow to compen-

sate for the limitations of the weak labels.

The use of a 2D patch-based segmentation network in our framework, rather than using complete 2D image slices, or more complex end-to-end 3D (Milletari *et al.*, 2016) or hybrid architectures (Isensee *et al.*, 2019), has been motivated by the need to increase the object-of-interest to image size ratio, as a way to mitigate the reduced performance of deep learning-based methods when the object of interest does not occupy an important portion of the input image. Furthermore, this simplifies the learning process: at a larger scale, the complexity and uniqueness of each brain vessel tree makes it difficult to learn common underlying patterns (Moriconi *et al.*, 2019), whereas, at a local scale, the characteristic patterns of vessels are similar between each other, allowing the network to learn them. Reducing the input size is a common strategy in learning-based vessel segmentation, beyond brain vessel tree segmentation (Kitrungrotsakul *et al.*, 2019; Koziński *et al.*, 2020). The poor results obtained by the 3D-Unet validate our choice for a simpler 2D patch-based segmentation network.

Alongside with the segmentation network, our framework includes a classification network that allows to automatically label training data. This network is trained using the same user-provided patch tags and it allows to classify image patches from unseen images that can be used to enlarge the original training set without the need for further user annotations. Our results show that the classifier network not only allows to enlarge the training dataset, but it can also act as a filter for noisy segmentations. Both scenarios are valid alternatives to increase segmentation accuracy without further user labeled training data, although the use of the noise filter requires a visual inspection step to identify low quality images. As part of our study, we investigated a set of different classification networks. Our results show that using networks specifically designed for medical image segmentation (Ronneberger *et al.*, 2015; Wang *et al.*, 2019), which we have adapted to the purpose of classification, leads to better results than those obtained with other general purpose well-established classification networks (He *et al.*, 2016; Simonyan and Zisserman, 2015). We consider this is an in-

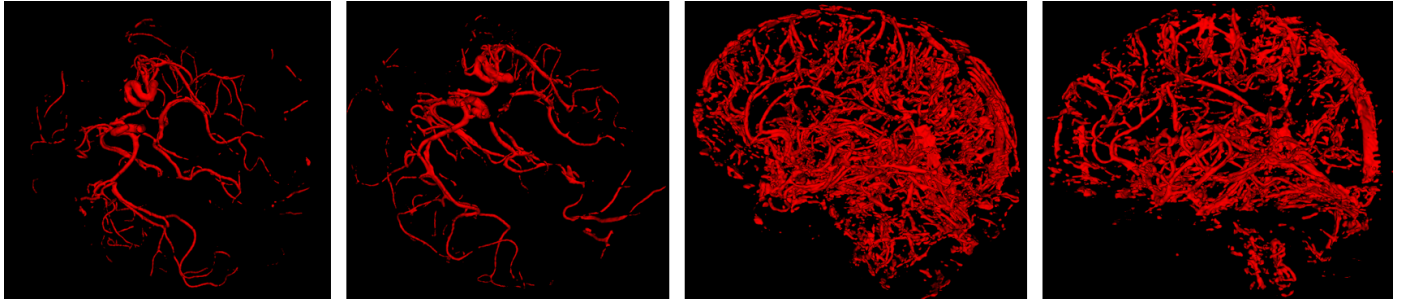


Fig. 11. 3D renderings of obtained segmentations in two TOF images (left) and two SWI (right).

interesting outcome that could motivate research to develop architectures specifically addressed to medical image classification problems. To date little work has explored this possibility (Mehta *et al.*, 2018). Issues such as the small size of the object of interest are not exclusive of vessel imaging and they are common to other medical imaging scenarios (Bejnordi *et al.*, 2017). Domain-specific classification networks could be designed to tackle these kind of problems.

We have evaluated the proposed framework in terms of its accuracy, measured by the DSC, and required annotation time. Our framework achieves performances equal to those of current state-of-the-art deep learning approaches for brain vessel segmentation (Livne *et al.*, 2019) and other well-established medical image segmentation networks, while reducing the annotation burden by nearly 80%. More classical approaches to vessel segmentation reported slightly lower performances than the two best performing deep learning methods, our proposed Vessel-CAPTCHA and the Vessel 2D-Unet (Livne *et al.*, 2019). However, to achieve these results classical approaches need of post-processing from highly skilled experts. Our promising results, with competitive accuracies and a significant reduction of the user-required effort, should enable the wider use of deep learning techniques for vessel segmentation. Although our work focuses on the brain vessel tree, we consider that the proposed framework is general enough that it can be easily extended to other vascular structures (Aughwane *et al.*, 2019), other tubular structures with complex networks to annotate (Zuluaga *et al.*, 2014a), and different image modalities. However, for some modalities the K-means algorithm used to synthesize pixel-wise labels can be limited. As an example, the coronary

vessel tree imaged with computed tomography angiography is likely to present calcified or lipid plaques that appear as hyper and hypo-intense objects, respectively (Zuluaga *et al.*, 2011). In the current setup, they would be segmented as a vessel (calcified plaques) or the background (lipid plaques). In such cases, there would be need to explore other self-supervised methods or the use of different types of image features (e.g. first and second order), which can cope with the characteristics of different vessel/tubular trees and image modalities.

Our experimental setup has included two different image modalities, TOF and SWI. This demonstrates the generality of the framework. Vessels in these two modalities are imaged with different appearance characteristics, hyper and hypo intense, respectively, and resolutions. SWI is capable of imaging vessels at a finer resolution, thus resulting in a larger number of visible but smaller vessels (Fig. 11). While the latter factor makes SWI a powerful tool for brain vessel analysis, it also makes it very challenging for accurate pixel-wise annotation. In a setting like this, the proposed annotation scheme becomes very relevant. However, due to the lack of pixel-wise annotations for SWI, the evaluation on this modality has been only qualitative. This points to an important problem: while our framework addresses the problem of annotation burden for learning-based model development, there is still the need of pixel-wise labels for the purpose of quantitative validation. This is an important issue that has been highlighted by other authors (Moccia *et al.*, 2018) and that hinders a faster progress in the field. Specific efforts should be directed towards the creation of more public benchmarks and platforms for 3D vessel segmentation, which are currently missing. As reported in (Moccia *et al.*, 2018), the majority of public

vessel segmentation datasets correspond to the retina, since 2D images are much simpler to annotate. While this problem is out of the scope our work, by simplifying the training data annotation process we indirectly contribute to a solution, particularly for learning-based methods. As pixel-wise annotations are not any more needed for training, efforts could be solely devoted to the annotation of a testing set. Moreover, if public benchmarks became widely available, or if a qualitative inspection was sufficient to validate a model, there would be no need of pixel-wise annotation at all to put in place a deep learning-based brain vessel segmentation model.

Obtaining high accuracies in vessel segmentation is a challenging task. For instance, we observed that our framework is capable of extracting larger vessels of very good quality in both modalities, but its performance diminishes for smaller ones. Although larger vessels are the most clinically relevant, there are certain diagnoses, which involve the assessment of small ones (Cortese *et al.*, 2018). In such scenarios, manual correction is often needed to improve initial automatic segmentation results. The proposed network could be extended to guide a user in the manual correction process. An idea to achieve this could be by using the disagreements between the segmentation and classification network predictions (i.e. 2D-WnetSeg segments a vessel in a patch classified as non-vessel or vice versa) as a measure of uncertainty. Since WnetSeg and PnetCl architectures are significantly different, we consider that they extract low-level and high-level features differently. As such, they are complementary to each other: if both agree on a prediction over a patch, the prediction can be considered as one of high confidence, whereas when there is a disagreement the patch can be suggested to the rater for revision.

Our main effort in this work has been directed towards a simplified annotation process and the development of mechanisms that can mitigate the negative effects of ‘simpler’ annotations to achieve performances comparable to the state-of-the-art. Nevertheless, we consider that there are different ways to achieve higher segmentation performance that could be explored. For instance, similarly to what has been proposed by (Koziński

et al., 2020; Phellan *et al.*, 2017), the annotations could be performed in different image planes. Currently, these are done in the axial plane. In addition, the Vessel-CAPTCHA allows for flexible annotations as, for some users, it is simpler to label vessels by following their trajectory. Now, all this information is discarded (see Fig. 2(e) and (g)), when in some cases it may have relevant content. The challenge here would be to identify when the patch annotations contain relevant information beyond the mere identification of the patch.

One last limitation of the current framework is related to the selection of the patch grid scheme. While it is convenient to present non-overlapping patches to the user, in some cases, this may degrade the framework’s performance. This is particularly true when the grid partition results in the split of vessels, in particular the smaller ones, across two or more patches causing them to lose their characteristic shape. The use of overlapping patches is a straightforward extension of this work that could reduce the number of misclassified vessels.

Acknowledgments

This work was supported by the French government, through the 3IA Côte d’Azur Investments in the Future project managed by the National Research Agency (ANR) (ANR-19-P3IA-0002), by the ANR JCJC project Fed-BioMed (19-CE45-0006-01), in part by the National Institute for Health Research University College London Hospitals Biomedical Research Centre (NIHR BRC UCLH/UCL High Impact), and by a Non-Clinical Postdoctoral Guarantors of Brain fellowship.

References

- Ahn, J., Kwak, S., 2018. Learning pixel-level semantic affinity with image-level supervision for weakly supervised semantic segmentation, in: 2018 IEEE/CVF Conference on Computer Vision and Pattern Recognition, pp. 4981–4990. doi:10.1109/cvpr.2018.00523.
- Aughwane, R., Schaaf, C., Hutchinson, J., Virasami, A., Zuluaga, M., Sebire, N., Arthurs, O., Vercauteren, T., Ourselin, S., Melbourne, A., David, A., 2019. Micro-CT and histological investigation of the spatial pattern of fetoplacental vascular density. *Placenta* 88, 36–43. doi:10.1016/j.placenta.2019.09.014.
- Bejnordi, B.E., Veta, M., van Diest, P.J., van Ginneken, B., Karssemeijer, N., Litjens, G., van der Laak, J.A.W.M., the CAMELYON16 Consortium, 2017. Diagnostic assessment of deep learning algorithms for detection of lymph node metastases in women with breast cancer. *JAMA* 318, 2199. doi:10.1001/jama.2017.14585.

- Can, Y.B., Chaitanya, K., Mustafa, B., Koch, L.M., Konukoglu, E., Baumgartner, C.F., 2018. Learning to segment medical images with scribble-supervision alone, in: *Deep Learning in Medical Image Analysis and Multimodal Learning for Clinical Decision Support*, pp. 236–244. doi:10.1007/978-3-030-00889-5_27.
- Cetin, S., Unal, G., 2015. A higher-order tensor vessel tractography for segmentation of vascular structures. *IEEE Transactions on Medical Imaging* 34, 2172–2185. doi:10.1109/tmi.2015.2425535.
- Chen, H., Qi, X., Yu, L., Heng, P.A., 2016. Dcan: Deep contour-aware networks for accurate gland segmentation, in: *2016 IEEE Conference on Computer Vision and Pattern Recognition*, pp. 2487–2496. doi:10.1109/CVPR.2016.273.
- Cheng, J.Z., Ni, D., Chou, Y.H., Qin, J., Tiu, C.M., Chang, Y.C., Huang, C.S., Shen, D., Chen, C.M., 24454 2016. Computer-aided diagnosis with deep learning architecture: Applications to breast lesions in US images and pulmonary nodules in CT scans. *Scientific Reports* 6. doi:10.1038/srep24454.
- Cheplygina, V., de Bruijne, M., Pluim, J.P., 2019. Not-so-supervised: A survey of semi-supervised, multi-instance, and transfer learning in medical Image Analysis. *Medical Image Analysis* 54, 280–296. doi:10.1016/j.media.2019.03.009.
- Çiçek, Ö., Abdulkadir, A., Lienkamp, S.S., Brox, T., Ronneberger, O., 2016. 3D U-net: Learning dense volumetric segmentation from sparse annotation, in: *Medical Image Computing and Computer-Assisted Intervention*, pp. 424–432. doi:10.1007/978-3-319-46723-8_49.
- Cortese, R., Magnollay, L., Tur, C., Abdel-Aziz, K., Jacob, A., De Angelis, F., Yiannakas, M.C., Prados, F., Ourselin, S., Yousry, T.A., et al., 2018. Value of the central vein sign at 3T to differentiate MS from seropositive NMOSD. *Neurology* 90, e1183–e1190. doi:10.1212/WNL.0000000000005256.
- Dai, J., He, K., Sun, J., 2015. Boxsup: Exploiting bounding boxes to supervise convolutional networks for semantic segmentation, in: *2015 IEEE Conference on Computer Vision and Pattern Recognition*, pp. 1635–1643. doi:10.1109/ICCV.2015.191.
- Deng, J., Dong, W., Socher, R., Li, L.J., Li, K., Fei-Fei, L., 2009. Imagenet: A large-scale hierarchical image database, in: *2009 IEEE Conference on Computer Vision and Pattern Recognition*, pp. 248–255. doi:10.1109/CVPR.2009.5206848.
- Dias, M., Monteiro, J., Estima, J., Silva, J., Martins, B., 2019. Semantic segmentation of high-resolution aerial imagery with w-net models, in: *Progress in Artificial Intelligence*. EPIA 2019, pp. 486–498. doi:10.1007/978-3-030-30244-3_40.
- Elson, J., Douceur, J.R., Howell, J., Saul, J., 2007. Asirra: a CAPTCHA that exploits interest-aligned manual image categorization, in: *ACM Conference on Computer and Communications Security*, pp. 366–374. doi:10.1145/1315245.1315291.
- Frangi, A.F., Niessen, W.J., Vincken, K.L., Viergever, M.A., 1998. Multiscale vessel enhancement filtering, in: *Medical Image Computing and Computer-Assisted Intervention*, pp. 130–137. doi:10.1007/bfb0056195.
- Hassouna, M.S., Farag, A., Hushek, S., Moriarty, T., 2006. Cerebrovascular segmentation from TOF using stochastic models. *Medical Image Analysis* 10, 2–18. doi:10.1016/j.media.2004.11.009.
- He, K., Zhang, X., Ren, S., Sun, J., 2016. Deep residual learning for image recognition, in: *2016 IEEE Conference on Computer Vision and Pattern Recognition*, pp. 770–778. doi:10.1109/CVPR.2016.90.
- Hong, S., Yeo, D., Kwak, S., Lee, H., Han, B., 2017. Weakly supervised semantic segmentation using web-crawled videos, in: *2017 IEEE Conference on Computer Vision and Pattern Recognition (CVPR)*, pp. 7322–7330. doi:10.1109/cvpr.2017.239.
- Isensee, F., Petersen, J., Klein, A., Zimmerer, D., Jaeger, P.F., Kohl, S., Wasserthal, J., Koehler, G., Norajitra, T., Wirkert, S., Maier-Hein, K.H., 2019. nnU-net: Self-adapting framework for u-net-based medical image segmentation, in: *Bildverarbeitung für die Medizin 2019*, pp. 22–22. doi:10.1007/978-3-658-25326-4_7.
- Kamnitsas, K., Ledig, C., Newcombe, V.F., Simpson, J.P., Kane, A.D., Menon, D.K., Rueckert, D., Glocker, B., 2017. Efficient multi-scale 3D CNN with fully connected CRF for accurate brain lesion segmentation. *Medical Image Analysis* 36, 61–78. doi:10.1016/j.media.2016.10.004.
- Kandil, H., Soliman, A., Taher, F., Mahmoud, A., Elmaghraby, A., El-Baz, A., 2018. Using 3-D CNNs and local blood flow information to segment cerebral vasculature, in: *2018 IEEE International Symposium on Signal Processing and Information Technology (ISSPIT)*, pp. 701–705. doi:10.1109/isspit.2018.8642676.
- Kitrungsakul, T., Han, X.H., Iwamoto, Y., Lin, L., Foruzan, A.H., Xiong, W., Chen, Y.W., 2019. VesselNet: A deep convolutional neural network with multi pathways for robust hepatic vessel segmentation. *Computerized Medical Imaging and Graphics* 75, 74–83. doi:10.1016/j.compmedimag.2019.05.002.
- Klepaczko, A., Szczypiński, P., Deistung, A., Reichenbach, J.R., Materka, A., 2016. Simulation of MR angiography imaging for validation of cerebral arteries segmentation algorithms. *Computer Methods and Programs in Biomedicine* 137, 293–309. doi:10.1016/j.cmpb.2016.09.020.
- Koziński, M., Mosinska, A., Salzmann, M., Fua, P., 2020. Tracing in 2D to reduce the annotation effort for 3D deep delineation of linear structures. *Medical Image Analysis* 60, 101590. doi:10.1016/j.media.2019.101590.
- Law, M.W.K., Chung, A.C.S., 2008. Three dimensional curvilinear structure detection using optimally oriented flux, in: *Proceedings of the European Conference on Computer Vision (ECCV)*, pp. 368–382. doi:10.1007/978-3-540-88693-8_27.
- Lesage, D., Angelini, E.D., Bloch, I., Funka-Lea, G., 2009. A review of 3D vessel lumen segmentation techniques: Models, features and extraction schemes. *Medical Image Analysis* 13, 819–845. doi:10.1016/j.media.2009.07.011.
- Li, X., Yang, F., Cheng, H., Liu, W., Shen, D., 2018. Contour knowledge transfer for salient object detection, in: *Proceedings of the European Conference on Computer Vision (ECCV)*, pp. 370–385. doi:10.1007/978-3-030-01267-0_22.
- Lin, D., Dai, J., Jia, J., He, K., Sun, J., 2016. ScribbleSup: Scribble-supervised convolutional networks for semantic segmentation, in: *2016 IEEE Conference on Computer Vision and Pattern Recognition*, pp. 3159–3167. doi:10.1109/CVPR.2016.344.
- Litjens, G., Kooi, T., Bejnordi, B.E., Setio, A.A.A., Ciompi, F., Ghafoorian, M., Van Der Laak, J.A., Van Ginneken, B., Sánchez, C.I., 2017. A survey on deep learning in medical image analysis. *Medical Image Analysis* 42, 60–88. doi:10.1016/j.media.2017.07.005.
- Livne, M., Rieger, J., Aydin, O.U., Taha, A.A., Akay, E.M., Kossen, T., Sobesky, J., Kelleher, J.D., Hildebrand, K., Frey, D., Madai, V.I., 2019. A U-net deep learning framework for high performance vessel segmentation in patients with cerebrovascular disease. *Frontiers in Neuroscience* 13. doi:10.3389/fnins.2019.00097.
- Lundervold, A.S., Lundervold, A., 2019. An overview of deep learning in medical imaging focusing on MRI. *Zeitschrift für Medizinische Physik* 29, 102–127. doi:10.1016/j.zemedi.2018.11.002.
- Luo, A., Li, X., Yang, F., Jiao, Z., Cheng, H., 2020. Webly-supervised learning for salient object detection. *Pattern Recognition* 103, 107308. doi:10.1016/j.patcog.2020.107308.
- Mehta, S., Mercan, E., Bartlett, J., Weaver, D., Elmore, J.G., Shapiro, L., 2018. Y-net: Joint segmentation and classification for diagnosis of breast biopsy images, in: *Medical Image Computing and Computer Assisted Intervention*, pp. 893–901. doi:10.1007/978-3-030-00934-2_99.
- Millertari, F., Navab, N., Ahmadi, S.A., 2016. V-net: Fully convolutional neural networks for volumetric medical image segmentation, in: *2016 Fourth International Conference on 3D Vision (3DV)*, pp. 565–571. doi:10.1109/3dv.2016.79.
- Moccia, S., Momi, E.D., Hadji, S.E., Mattos, L.S., 2018. Blood vessel segmentation algorithms — review of methods, datasets and evaluation metrics. *Computer Methods and Programs in Biomedicine* 158, 71–91. doi:10.1016/j.cmpb.2018.02.001.
- Moriconi, S., Zuluaga, M.A., Jager, H.R., Nachev, P., Ourselin, S., Cardoso, M.J., 2019. Inference of cerebrovascular topology with geodesic minimum spanning trees. *IEEE Transactions on Medical Imaging* 38, 225–239. doi:10.1109/tmi.2018.2860239.
- Ni, J., Wu, J., Wang, H., Tong, J., Chen, Z., Wong, K.K., Abbott, D., 2020. Global channel attention networks for intracranial vessel segmentation. *Computers in Biology and Medicine* 118, 103639. doi:10.1016/j.compbiomed.2020.103639.
- Pepe, A., Schussnig, R., Li, J., Gsaxner, C., Chen, X., Fries, T.P., Egger, J., 2020. IRIS: interactive real-time feedback image segmentation with deep learning, in: *Proc. SPIE Medical Imaging 2020: Biomedical Applications in Molecular, Structural, and Functional Imaging*, p. 113170R. doi:10.1117/12.2551354.
- Phellan, R., Peixinho, A., Falcão, A., Forkert, N.D., 2017. Vascular segmentation in TOF MRA images of the brain using a deep convolutional neural network, in: *Intravascular Imaging and Computer Assisted Stenting, and Large-Scale Annotation of Biomedical Data and Expert Label Synthesis*,

- pp. 39–46. doi:10.1007/978-3-319-67534-3_5.
- Radbruch, A., Mucke, J., Schweser, F., Deistung, A., Ringleb, P.A., Ziener, C.H., Roethke, M., Schlemmer, H.P., Heiland, S., Reichenbach, J.R., Bendszus, M., Rohde, S., 2013. Comparison of susceptibility weighted imaging and TOF-angiography for the detection of thrombi in acute stroke. *PLoS ONE* 8, e63459. doi:10.1371/journal.pone.0063459.
- Rajchl, M., Lee, M.C.H., Oktay, O., Kamnitsas, K., Passerat-Palmbach, J., Bai, W., Damodaram, M., Rutherford, M.A., Hajnal, J.V., Kainz, B., Rueckert, D., 2017. DeepCut: Object segmentation from bounding box annotations using convolutional neural networks. *IEEE Transactions on Medical Imaging* 36, 674–683. doi:10.1109/tmi.2016.2621185.
- Rempfler, M., Schneider, M., Ielacqua, G.D., Xiao, X., Stock, S.R., Klohs, J., Székely, G., Andres, B., Menze, B.H., 2015. Reconstructing cerebrovascular networks under local physiological constraints by integer programming. *Medical Image Analysis* 25, 86–94. doi:10.1016/j.media.2015.03.008.
- Robben, D., Türetken, E., Sunaert, S., Thijs, V., Wilms, G., Fua, P., Maes, F., Suetens, P., 2016. Simultaneous segmentation and anatomical labeling of the cerebral vasculature. *Medical Image Analysis* 32, 201–215. doi:10.1016/j.media.2016.03.006.
- Ronneberger, O., Fischer, P., Brox, T., 2015. U-net: Convolutional networks for biomedical image segmentation, in: *Medical Image Computing and Computer-Assisted Intervention*, pp. 234–241. doi:10.1007/978-3-319-24574-4_28.
- Sato, Y., Nakajima, S., Atsumi, H., Koller, T., Gerig, G., Yoshida, S., Kikinis, R., 1997. 3d multi-scale line filter for segmentation and visualization of curvilinear structures in medical images, in: *First Joint Conference Computer Vision, Virtual Reality and Robotics in Medicine and Medical Robotics and Computer-Assisted Surgery*, pp. 213–222. doi:10.1007/bfb0029240.
- Schlegl, T., Waldstein, S.M., Vogl, W.D., Schmidt-Erfurth, U., Langs, G., 2015. Predicting semantic descriptions from medical images with convolutional neural networks, in: *Information Processing in Medical Imaging*, pp. 437–448. doi:10.1007/978-3-319-19992-4_34.
- Setio, A.A.A., Ciampi, F., Litjens, G., Gerke, P., Jacobs, C., van Riel, S.J., Wille, M.M.W., Naqibullah, M., Sanchez, C.I., van Ginneken, B., 2016. Pulmonary nodule detection in CT images: False positive reduction using multi-view convolutional networks. *IEEE Transactions on Medical Imaging* 35, 1160–1169. doi:10.1109/tmi.2016.2536809.
- Shelhamer, E., Long, J., Darrell, T., 2017. Fully convolutional networks for semantic segmentation. *IEEE Transactions on Pattern Analysis and Machine Intelligence* 39, 640–651. doi:10.1109/tpami.2016.2572683.
- Simonyan, K., Zisserman, A., 2015. Very deep convolutional networks for large-scale image recognition, in: *3rd International Conference on Learning Representations, Conference Track Proceedings*. URL: <http://arxiv.org/abs/1409.1556>.
- Taher, F., Soliman, A., Kandil, H., Mahmoud, A., Shalaby, A., Gimelfarb, G., El-Baz, A., 2020. Accurate segmentation of cerebrovasculature from TOF-MRA images using appearance descriptors. *IEEE Access* 8, 96139–96149. doi:10.1109/access.2020.2982869.
- von Ahn, L., Blum, M., Hopper, N.J., Langford, J., 2003. CAPTCHA: Using hard AI problems for security, in: *Advances in Cryptology – EUROCRYPT 2003*, pp. 294–311. doi:10.1007/3-540-39200-9_18.
- von Ahn, L., Dabbish, L., 2004. Labeling images with a computer game, in: *Proceedings of the SIGCHI Conference on Human Factors in Computing Systems*, pp. 319–326. doi:10.1145/985692.985733.
- Wang, G., Li, W., Zuluaga, M.A., Pratt, R., Patel, P.A., Aertsen, M., Doel, T., David, A.L., Deprest, J., Ourselin, S., Vercauteren, T., 2018. Interactive medical image segmentation using deep learning with image-specific fine tuning. *IEEE Transactions on Medical Imaging* 37, 1562–1573. doi:10.1109/tmi.2018.2791721.
- Wang, G., Zuluaga, M.A., Li, W., Pratt, R., Patel, P.A., Aertsen, M., Doel, T., David, A.L., Deprest, J., Ourselin, S., Vercauteren, T., 2019. DeepGeoS: A deep interactive geodesic framework for medical image segmentation. *IEEE Transactions on Pattern Analysis and Machine Intelligence* 41, 1559–1572. doi:10.1109/tpami.2018.2840695.
- Wang, G., Zuluaga, M.A., Pratt, R., Aertsen, M., David, A.L., Deprest, J., Vercauteren, T., Ourselin, S., 2015. Slic-seg: Slice-by-slice segmentation propagation of the placenta in fetal MRI using one-plane scribbles and online learning, in: *Medical Image Computing and Computer-Assisted Intervention*, pp. 29–37. doi:10.1007/978-3-319-24574-4_4.
- Wang, J., Chung, A.C.S., 2020. Higher-order flux with spherical harmonics transform for vascular analysis, in: *Medical Image Computing and Computer Assisted Intervention*, pp. 55–65. doi:10.1007/978-3-030-59725-2_6.
- World Health Organization, 2020. Global health estimates. URL: <https://www.who.int/data/global-health-estimates>.
- Zhao, S., Zhou, M., Tian, Y., Xu, P., Wu, Z., Deng, Q., 2015. Extraction of vessel networks based on multiview projection and phase field model. *Neurocomputing* 162, 234–244. doi:10.1016/j.neucom.2015.03.048.
- Zuluaga, M.A., Hush, D., Leyton, E.J.D., Hoyos, M.H., Orkisz, M., 2011. Learning from only positive and unlabeled data to detect lesions in vascular CT images, in: *Medical Image Computing and Computer-Assisted Intervention*, pp. 9–16. doi:10.1007/978-3-642-23626-6_2.
- Zuluaga, M.A., Orkisz, M., Dong, P., Pacureanu, A., Gouttenoire, P.J., Peyrin, F., 2014a. Bone canalicular network segmentation in 3D nano-CT images through geodesic voting and image tessellation. *Physics in Medicine and Biology* 59, 2155–2171. doi:10.1088/0031-9155/59/9/2155.
- Zuluaga, M.A., Rodionov, R., Nowell, M., Achhala, S., Zombori, G., Cardoso, M.J., Miserocchi, A., McEvoy, A.W., Duncan, J.S., Ourselin, S., 2014b. SEEG trajectory planning: Combining stability, structure and scale in vessel extraction, in: *Medical Image Computing and Computer-Assisted Intervention*, pp. 651–658. doi:10.1007/978-3-319-10470-6_81.